Investigation of ultrafast photoinduced processes for salicylidene aniline in solution and gas phase: toward a general photo-dynamical scheme†

Michel Sliwa,*[a] Nicolas Mouton,[a] Cyril Ruckebusch,[a] Lionel Poisson,*[b] Abdenacer Idrissi,[a] Stéphane Aloïse,[a] Ludovic Potier,[a] Julien Dubois,[a] Olivier Poizat[a] and Guy Buntinx[a]

Received 30th December 2009, Accepted 16th February 2010
First published as an Advance Article on the web 3rd March 2010
DOI: 10.1039/b9pp00207c

Photodynamics of 2-hydroxybenzylideneaniline (photochromic salicylidene aniline SAOH) and *N*-(2-methoxybenzylidene)aniline (SAOMe) are studied by steady state and transient optical spectroscopy in solution and gas phase at different excitation wavelengths (266, 355 and 390 nm). Two competitive processes are observed from the enol* excited state: on one hand a rotation to get a twisted-enol, and on the other hand an excited state intramolecular proton transfer (ESIPT) followed by a *cis–trans* isomerisation to get the *trans*-keto photochromic product. For the first time both processes are characterized at an ultrashort time scale for salicylidene aniline. Resolution of the spectrokinetic data is achieved by multivariate curve resolution and attribution of the intermediate species recovered is performed in comparison with the results obtained for SAOMe, which can only undergo enol rotational isomerisation. It shows that ESIPT and rotation to the twisted-enol for SAOH occur within 100 fs, as predicted by recent quantum dynamical simulations, with an efficiency ratio dependent on the excitation wavelength. Therefore a general photoinduced mechanism for salicylidene aniline is drawn.

A Introduction

Photochromic and photo-switchable materials have been intensively studied for several years for their potential applications in optical devices, from ophthalmic lenses to optical memories or fluorescent switches.[1–4] Recently, it was demonstrated that photo-switchable fluorescent single molecules and nanoparticles can be used to probe biological processes under optical microscopes with an unprecedented nanometre spatial resolution.[5–7] Molecules for which the photochromism involves an excited state proton transfer are of particular interest since the kinetics of this transfer is valuable for fast switching applications and very attractive from a fundamental point of view.[8] During the last decade, particular attention has been paid to anils, such as salicylidene-anilines, salicylidene-aminopyridines, and related Schiff bases.[9–20] The results obtained using several ultrafast spectroscopic techniques in solution, in addition to gas and crystalline phases, have completed the overview of the photo-reaction of anils, which started half a century ago.[21–40] The mechanism now generally accepted is summarized in Scheme 1.

From a historical perspective, 2-hydroxybenzylideneaniline (or salicylidene aniline, SAOH) has been studied for more than a century[41–44] and is nowadays the most well-known photochromic anil. The excited state intramolecular proton transfer (ESIPT) of this compound in acetonitrile has been recently described in good detail using femtosecond fluorescence up-conversion[40] or transient absorption experiments.[37] Excitation of the stable enol form is followed by (1) ESIPT, yielding a vibrationally hot *cis*-keto* form within 50 fs, which (2) relaxes to the fluorescent relaxed (cold) *cis*-keto* species in 500 fs, then (3) leads in about 6 ps to both the *cis*-keto ground state (radiative decay) and the final *trans*-keto photo-product (radiationless process). However, the rising kinetics of the latter could not be estimated due to a strong overlap of its absorption spectrum with those of the intermediate species. Accordingly, only the lifetime of the *cis*-keto* could be measured.

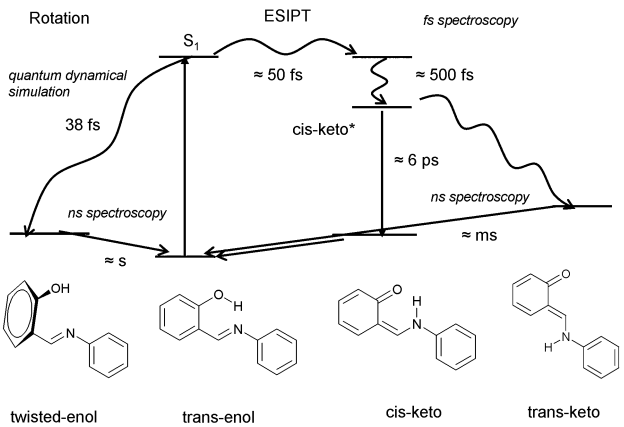

Scheme 1 Overall photoinduced processes for SAOH reported in the literature.

Several other aspects of the ultrafast enol* reactivity still require experimental assessment, including the evidence of a competitive deactivation pathway and the possible contribution of different structural isomers of the enol, *cis*-keto, and *trans*-keto, species with either zwitterionic or quinoidal configurations depending

[a]*Laboratoire de Spectrochimie Infrarouge et Raman (UMR 8516 CNRS), Université de Lille 1 Sciences et Technologies, Bât. C5, 59655, Villeneuve d'Ascq Cedex, France. E-mail: michel.sliwa@univ-lille1.fr; Fax: +33 3 20 43 67 55; Tel: +33 3 20 33 63 53*
[b]*Laboratoire Francis PERRIN, Bât. 522, CEA/DSM/IRAMIS/SPAM-CNRS URA 2453, 91191, Gif-sur-Yvette Cedex, France. E-mail: lionel.poisson@cea.fr; Fax: +33 1 69 08 84 46; Tel: +33 1 69 08 51 61*

† Electronic supplementary information (ESI) available: Spectrum of the twisted enol for SAOMe and ultrafast time-resolved experiments for SAOH after 390 nm excitation. See DOI: 10.1039/b9pp00207c

on the environment. From X-ray data, the stable SAOH enol is the *trans*-enol (or *anti*-enol) form.[45] Nanosecond flash photolysis studies in solution suggested that a *trans–cis* enol isomerisation is photo-induced in addition to ESIPT.[46,47] In fact, a *trans*-enol bleaching component was still observed after the complete decay of the *trans*-keto photo-product absorption and accounted for by the existence of a long-lived *cis*-enol (or *syn*-enol) isomer (lifetime 1 s). Indeed recent time-dependent density functional theory and quantum dynamical calculations predicted that two competing processes occur in the first excited singlet (π–π*) planar enol* state: ESIPT within 50 fs, in agreement with the experimental value,[37,40] and deactivation through a S_1/S_0 conical intersection leading within 38 fs to a twisted-enol ground state form characterized by a rotation around the double C–N bond (N–C–C–C–O dihedral angle of about 90°, see Scheme 1).[48] This twisted-enol S_0 species is equivalent to the *cis*-enol tautomer observed by nanosecond flash photolysis. However none of the ultrafast transient experiments performed on SAOH, neither in solution nor in gas phase, ever evidenced the formation of this twisted-enol isomer predicted by quantum chemical calculations or the *cis*-enol observed by nanosecond flash photolysis experiments.[35,37,40,49]

Following the progress toward a general photodynamical scheme of the ultrafast photoinduced processes in anils, we report in this article (i) nanosecond transient absorption experiments on SAOH in acetonitrile at two different excitation wavelengths, 355 and 266 nm, (ii) femtosecond experiments at 266 nm in acetonitrile in order to observe the UV region and the ground state depopulation signal, and (iii) femtosecond time-resolved mass spectroscopy experiments in the gas phase at 266 nm excitation to have a better resolution at ultrashort time scales. To complement this, *N*-(2-methoxybenzylidene)aniline (SAOMe, Fig. 1), which can only undergo planar- to twisted-enol isomerization, is used as a reference compound to help in understanding the SAOH reactivity. All our results are compared to those obtained with 390 nm excitation to compare the different decay pathways (ESI, 2†). Soft-modeling data analysis is applied to resolve transient absorption spectroscopy. Multivariate curve resolution (MCR)[50–52] enables strongly overlapping transient spectra to be unravelled, which provides better insights into the reaction mechanism. In particular, the characteristic time for the formation of *trans*-keto photo-product will be readily assessed. To the best of our knowledge, it is the first time that ultrafast transient absorption experiments after 266 nm excitation are reported for SAOH and SAOMe. Our results demonstrate the existence of both ESIPT and excited state enol rotation within 100 fs, in good agreement with the recent quantum chemical calculations.[48] These are the first experiments leading to a full characterization of the ESIPT and enol rotation photoinduced processes in SAOH. Therefore an overall reaction scheme will be drawn and discussed in detail.

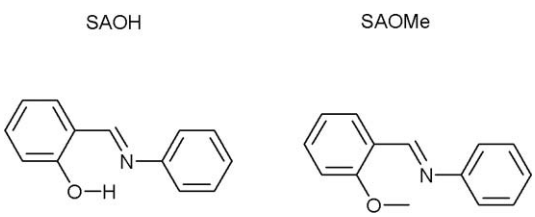

Fig. 1 Molecular structures of SAOH and SAOMe.

B Results

B.1 Steady state absorption/fluorescence

Stationary absorption and fluorescence spectra, excited at 355 nm and 266 nm, are shown in Fig. 2 for SAOH and SAOMe in acetonitrile. Two main absorption bands are observed at 336 and 268 nm for SAOH and at 325 and 264 nm for SAOMe. Quantum calculations performed with the use of Gaussian03 predict a *trans*-enol ground state geometry for the two molecules, with the phenol ring and the imine part in the same plane and twisted relative to the phenyl ring plane by 33° (SAOH) and 38° (SAOMe). For SAOMe the methyl group is out of the phenol ring plane. The vertical excitation energies (corrected values) are 3.546 eV (350 nm) and 4.773 eV (260 nm) for SAOH and 3.793 eV (327 nm) and 4.672 eV (266 nm) for SAOMe. In agreement with previous reports, these transitions have (π–π*) and (n–π*) character, respectively.[48,53] All fluorescence spectra were obtained for the same absorbance value at the excitation wavelength, allowing comparison of their relative intensity. For 355 nm excitation, SAOH shows a weak broad-band fluorescence (quantum yield about 10^{-4}) from 430 to 700 nm with a maximum at 533 nm exhibiting a strong Stoke shift characteristic of the *cis*-keto* form. A weak shoulder at 420 nm is usually assigned to the excited enol species.[37] Another shoulder is observed at 480 nm. It corresponds to the position of the very weak fluorescence band observed for SAOMe, for which the lack of any emission above 550 nm is consistent with the fact that ESIPT is forbidden. The ~480 nm emission in both SAOMe and SAOH is thus attributed to an excited enol* form. The strong bathochromic shift noticed for this fluorescence reveals a notably different geometry of the excited state in comparison to that of the ground state. For 266 nm excitation, the SAOH and SAOMe fluorescence shows mainly a sharp band at 330 nm, in agreement with the literature,[33] and a very weak signal at the position of the *cis*-keto*. The intensity ratio between these two bands leads to the conclusion that the ESIPT is not the predominant pathway and the relaxation of higher excited states not only goes through the same S_1 enol* excited state reached with 355 nm excitation. Quantum chemical calculations of the potential energy curves as a function of the N–C–C–C–O torsion angle predicted different minima for the first four enol excited states of SAOH.[48] Thus relaxation after 266 nm excitation can proceed through different pathways and can lead to different S_1 enol* geometries than with the 355 nm

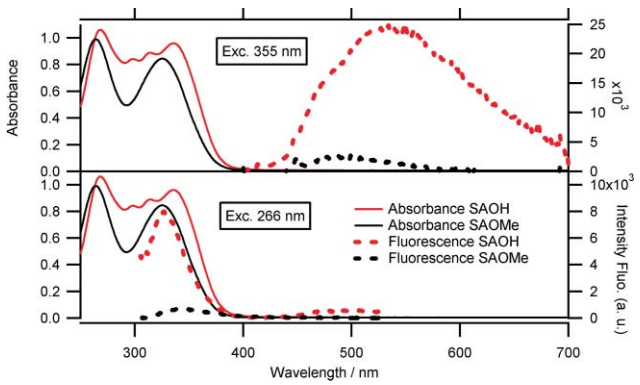

Fig. 2 Steady state absorption (full line) and fluorescence (dashed line) spectra for SAOH (red) and SAOMe (black) in acetonitrile upon excitation at 355 nm (top) and 266 nm (bottom).

excitation. This will be also pointed out with nanosecond transient absorption results.

B.2 Nanosecond photolysis

Fig. 3 shows nanosecond transient absorption spectra of SAOMe and SAOH in acetonitrile after 266 nm and 355 nm excitations at different time delays. As expected, a negative signal at 330 nm is mainly observed for SAOMe and a very weak positive absorption band covering all the visible part with a maximum at about 450 nm (ESI, 1†). The negative signal is assigned to the ground state bleach and shows a 5 nm bathochromic shift of its maximum with respect to the steady state absorption maximum of lowest energy. This persistent ground state bleach, associated to the quasi-absence of absorption in the visible range, reveals the presence of a long-lived photo-product that is likely the SAOMe twisted-enol. In fact, the break of the electronic delocalisation between the two rings in the twisted-enol geometry is expected to shift the absorbance to shorter UV wavelengths compared to the starting *trans*-enol. The presence of this blue-shifted absorption, superimposed on the *trans*-enol bleach signal, can explain the bathochromic shift observed for the latter. As seen in Fig. 3, no bleach recovery is observed in the time window of the nanosecond photolysis experiment. However, no trace of the presence of the twisted-enol could be seen in the stationary spectra recorded under continuous irradiation. We thus concluded that the twisted-enol goes back to the stable *trans*-enol within 1 s for both excitations. The same spectra are obtained with 355 (not shown) and 266 nm excitation wavelengths. From the intensity of the bleach signal measured just after the excitation, the quantum yield for the formation of the twisted-enol can be estimated on the basis of the measured reference signal for the triplet state of benzophenone knowing the stationary absorption coefficients for SAOMe (see Experimental section). Independently of the excitation wavelength, a quantum yield of about 45% is found.

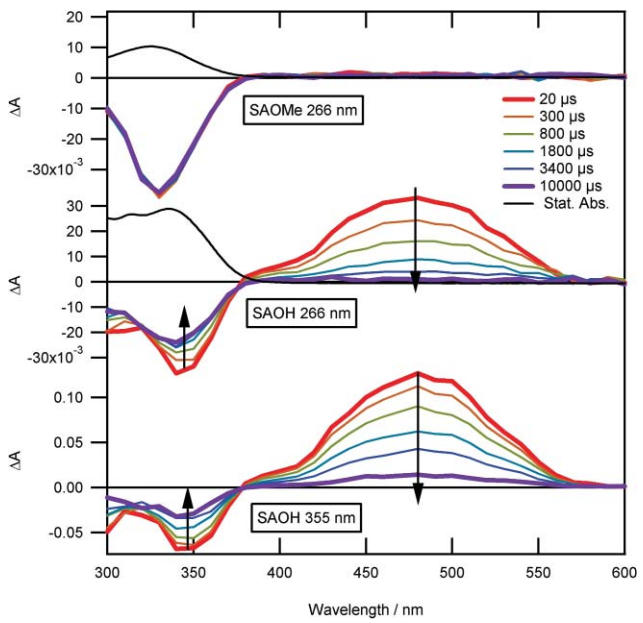

Fig. 3 Stationary absorption spectra of enol (black line, Stat. Abs. in the legend) and nanosecond transient differential spectra at different time delays (nanosecond photolysis) for SAOH and SAOMe in acetonitrile after 266 and 355 nm excitation.

The SAOH transient spectra exhibit, in addition to the ground state depopulation band, a positive band from 380 to 600 nm with a maximum at about 480 nm observed for both excitation wavelengths. In agreement with previous reports,[46,47] the transient absorption contribution is unambiguously assigned to the *trans*-keto photo-product and the negative band to the *trans*-enol ground state depopulation (with a 5 nm bathochromic shift relative to the steady state absorption maximum). The *trans*-keto photo-product and the ground state bleach signals decay with similar time constants: 2.5 ms (33%) and 0.7 ms (66%) upon 266 nm excitation, and 3.8 ms (66%) and 0.94 ms (33%) at 355 nm. These decay kinetics are insensitive to the presence of oxygen and the sample concentration. The bi-exponential character of the decay can be attributed to the formation of two distinct *trans*-keto isomers with similar spectral signatures but different thermal stabilities, and with relative efficiencies dependent on the excitation wavelength. After the entire decay of the *trans*-keto absorption, the remaining spectrum is essentially a bleach component analogous to that observed for SAOMe and thus likely due to the twisted-enol isomer. The twisted-enol leads back to *trans*-enol within ~1 s. The intensity of the residual bleach (measured at 340 nm) relative to its initial intensity just after the excitation is 66% at 266 nm and 45% at 355 nm. A global quantum yield for the formation of the twisted-enol and the *trans*-keto photo-product was calculated in a similar way than for SAOMe. A quantum yield of about 25% and 35% was found for 355 nm and 266 nm excitation. Therefore, it can be concluded that 355 nm excitation leads in majority to the ESIPT process (14% *trans*-keto *vs.* 11% twisted-enol photo-product), whereas 266 nm excitation leads in majority to the enol rotation process (12% *trans*-keto *vs.* 23% twisted-enol photo-product). Similar results were recently found for a derivative of SAOH.[18] Using quantum chemical calculations,[48] this result can be explained by involving a different geometry of the excited enol* (already twisted, which favors enol rotation) in the relaxation after 266 nm excitation than the one obtained after 355 nm excitation (planar enol*).

B.3 Femtosecond studies

B.3.1 Investigation in the gas phase. Time-resolved mass spectroscopy and photo-electron spectroscopy of SAOMe were performed with 266 nm laser pump and 792 nm or 399 nm probes (Fig. 4). Several specificities of the experimental results obtained can be enlightened. The first concerns the parent mass, which does not show any kinetic behavior. The laser probe ionizes the molecule in a multiphoton ionization process. This ionization process is known to be followed by a strong fragmentation since the broad-spectrum of the femtosecond laser favors the resonant autoionization process from the direct ionization.[54] The energy introduced in the molecule is large enough to induce the fragmentation of the molecular ion. In the present case, the fragment observed arises mainly from the loss of a phenyl or substituted phenyl ring from the molecule. Since the final product issues from the reaction dynamics in the autoionizing or ionic state, the masses are usually difficult to attribute properly. Indeed the mass distribution arises from several processes, among them a statistical fragmentation controlled by the thermodynamics of the ion or the direct fragmentation of the ion. The mass spectrum also does not give any information on the reaction dynamics of interest. Contrary to this, the relative

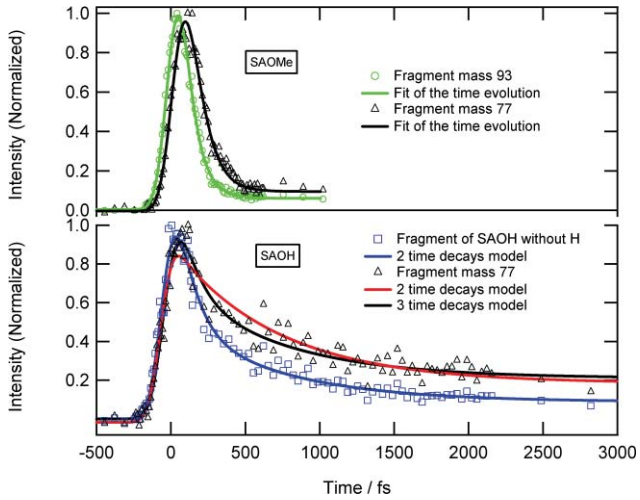

Fig. 4 Top: Time evolution of the SAOMe relaxation followed on fragments of mass 93 and mass 77. Bottom: Relaxation of the SAOH molecules followed on the fragments of mass corresponding to the loss of hydrogen, and to the formation of mass 77. Two fits are displayed for the latter mass.

intensity of the fragment mass documents the open channels at the ionizing time of the excited molecule. Indeed, while the excited molecule explores its potential energy surface, the relative contribution of the ionization mechanisms changes in correlation with the projection of the wavepacket to the ionic states by the probe laser. In particular, a new fragmentation can be opened. The time evolution of the fragment peaks is also correlated with the dynamics of the excited state.

The second distinctive feature concerns the time evolution of all the fragments, which shows a sequential first-order kinetic model $A \rightarrow B \rightarrow C$ with characteristic time constants being 40 ± 10 fs and 90 ± 20 fs, respectively. As usual, the determination of almost identical time constants should be regarded very cautiously. In the present case, their determination can be considered unambiguous since the fragment of mass 77 shows only the second component of the dynamics in comparison, for example, with fragment of mass 93 (Fig. 4). It corresponds, in the excited molecule, to a change leading to the opening of a new fragmentation channel (increase of the internal energy or change in the selection rules for the ionization can be a reason for that). The first step of the proposed mechanism is typical of a S_n to S_1 relaxation. As only rotation is possible in the case of SAOMe, the decay of S_1 excited state to twisted-enol is then achieved in less than 100 fs.

The electronic excitation of SAOH at 266 nm shows surprisingly longer dynamics. Indeed, the mass peak corresponding, for example, to the loss of hydrogen in the ionic state shows two time decay dynamics of 40 ± 10 fs and 700 ± 100 fs. The two characteristic times are attributed respectively to ESIPT and to the first relaxation of the *cis*-keto*, which is in agreement with experiments in solution.[40] As well as for the SAOMe molecule, the fragment of mass 77 does not show the first decay time. The decay is more complex, and has other components than the expected 700 ± 100 fs one mentioned above. Indeed, the result of the fit is strongly improved when a third contribution of characteristic time 110 ± 30 fs is added. This third component is assigned to the decay of a planar excited state to the twisted-enol, again comparing with SAOMe results. The attribution of these kinetics will be further discussed and compared with the results obtained in solution.

B.3.2 Investigations in acetonitrile solution.

B.3.2.1 SAOMe after 266 nm excitation. Fig. 5 shows the transient absorption spectra of SAOMe measured in acetonitrile following femtosecond excitation at 266 nm for time delays in the range 0 to 25 ps. The instrumental response function is about 300 fs and, in this time domain, two main bands are growing with the excitation pulse: a broad absorption band covering the 360–650 nm domain and a weak negative band in the 310–360 nm domain. The latter shows a bathochromic shift and the former, which is broad at the beginning, leads to a sharper maximum at 400 nm and a long red tail. The negative band is assigned undoubtedly to ground state bleach. The early broad absorption can be assigned to a first excited state reached by the Franck–Condon transition (upper state S_n or hot S_1 enol*) and the 400 nm band to the enol* S_1 state. Then the bands decay in 500 fs. The absence of an isosbestic point indicates that the apparent increase of the ground state bleach is indeed due to the decrease of the broad absorption band which is partially superimposed to the bleach band. This 500 fs kinetics can be assigned to the decay of S_1 enol* to the twisted-enol ground state through a conical intersection, as suggested by quantum chemical calculations[48] and the above-mentioned gas phase experiments. The corresponding 90 ± 20 fs gas phase dynamics is probably slowed down in solution by the dynamics of reorganization of the dipolar solvant. During its decay, the 400 nm band keeps narrowing until 1.5 ps and shifts to a maximum at 390 nm while the red tail contribution almost disappears. During this process the ground state bleach band does not change. Finally, the 390 nm absorption band disappears in 25 ps and leads to a flat absorption in the 380–550 nm range, whereas the ground state bleach decays simultaneously to a stationary value. This spectrum remains mainly constant from 25 ps and can be assigned to the twisted-enol (*syn*-enol) by analogy with the above-mentioned nanosecond flash photolysis results.

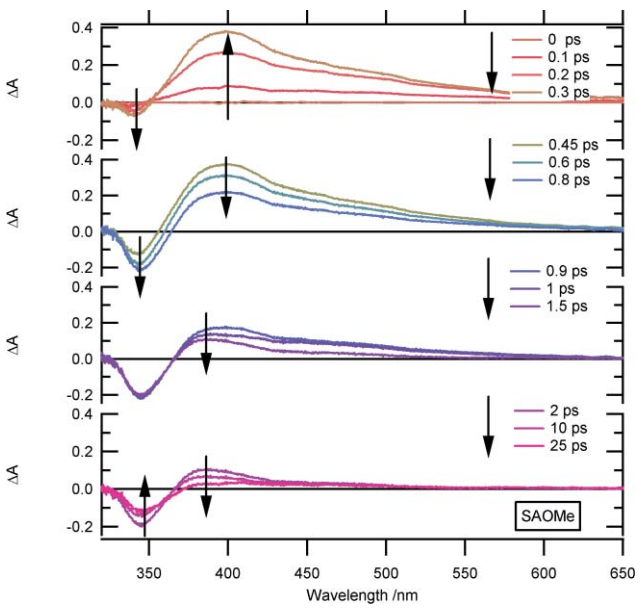

Fig. 5 Transient absorption spectra of SAOMe in acetonitrile obtained for different time delays after 266 nm excitation (3 mJ cm^{-2}).

The intermediate 390 nm band can be tentatively explained by the existence of another unstable ground state enol form which relaxes to the stable *trans*-enol much more rapidly than the twisted-enol. Its geometry is thus quite close to the *trans*-enol geometry and named "unstable *trans*-enol" in the following of the discussion. The narrowing step is in favor of a cooling step before reaching this unstable *trans*-enol. The early kinetic analysis is complex as many species with strongly overlapping spectra are involved (S_1, unstable *trans*-enol, twisted-enol, ground state depopulation, *etc.*). Thus, MCR soft modelling analysis[55,56] was attempted to get a better knowledge of the SAOMe relaxation. The constraints applied during the MCR-ALS (see Experimental section) optimization were non-negativity and unimodality of the time-dependent concentration profiles, and normalization to unit surface area for the transient spectra. The results obtained for the four components extracted during the resolution are shown in Fig. 6 for pure transient spectra and corresponding time-dependent concentration, respectively. The fitting error was evaluated globally (lack of fit, lof = 2.43%) and the distribution of the residuals was checked. Two different spectra (red and green) are found to increase first and disappear within 1 ps. It confirms our first analysis that two species, one with a broad positive band and another one with a maximum at about 400 nm, appear within the excitation. The broad one (red spectrum) seems to appear first, but there is no clear evidence that one is the precursor of the other one. The first broad spectrum (red spectrum) is assigned to absorption of higher excited states and the green one to S_1 enol* absorption. It is quite rare to have such a long lifetime for higher excited states. However this is in agreement with the weak fluorescence observed from S_2 for SAOMe (Fig. 2). Then red and green spectra lead to both blue and black spectra within 1.5 and 0.5 ps. These processes can be assigned respectively to the formation of the unstable *trans*-enol (positive band with a maximum at 385 nm, blue spectrum) and twisted-enol (weak broad positive band, black spectrum) from enol*, respectively. 266 nm excitation opens two pathways, the first giving the twisted-enol within 500 fs and the second giving the unstable *trans*-enol within 1.5 ps (fit of the increasing time of concentration profile for blue spectrum) *via* a cooling process characterized by a strong shift of its maximum. Then the unstable *trans*-enol (blue spectrum) recovers the final stable *trans*-enol in 14 ps.

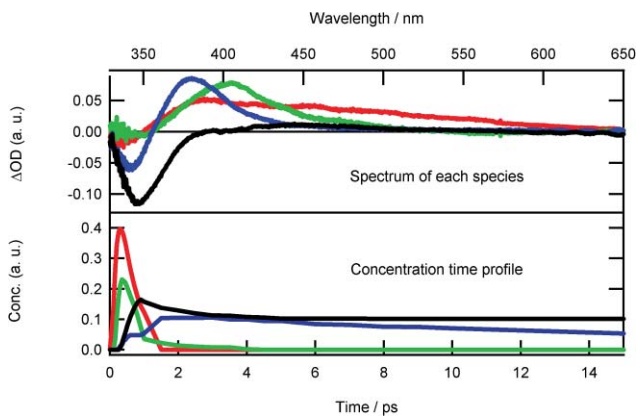

Fig. 6 (Top) Spectra and (bottom) time-dependent concentration profiles obtained from MCR-ALS for transient absorption spectra of SAOMe in acetonitrile for different time delays after 266 nm excitation.

B.3.2.2 SAOH after 266 nm excitation. Fig. 7 shows the transient absorption spectra of SAOH measured in acetonitrile following excitation at 266 nm for time delays from 0 to 25 ps. Two main bands are growing with the excitation pulse: a broad absorption band covering the 360–600 nm domain and a weak negative bleach band in the 310–360 domain. In addition, a weak negative band also starts to grow above 580 nm. From 300 fs to 800 fs the ground state bleach stays constant while both the absorption and 550–650 nm negative components continue to increase. At 800 fs the absorption band has a maximum at 410 nm and a shoulder at 500 nm. Then the 550–650 nm negative band disappears together with the 410 nm absorption to give at 8 ps three main components: the almost unchanged bleach signal, a broad absorption covering the 360–420 nm domain with a rough maximum around 380 nm, and a band covering the 450–600 nm domain and peaking at 480 nm. Finally, the 360–420 nm band disappears in 25 ps concomitantly with the partial decay of the bleach band, whereas the 480 nm absorption remains stable. After 25 ps the transient spectrum is stable and similar to the one obtained by the nanosecond transient absorption experiment.

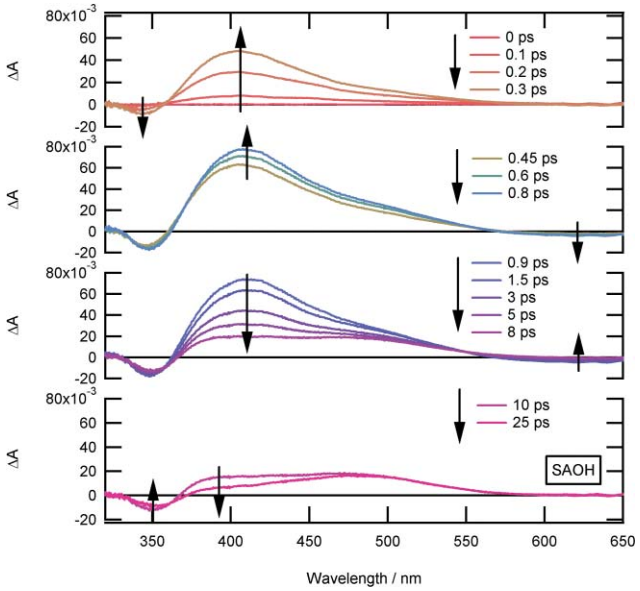

Fig. 7 Transient absorption spectra of SAOH in acetonitrile obtained for different time delays after 266 nm excitation (3 mJ cm^{-2}).

Taking into account the results with 390 nm excitation (ESI, 2†), the negative band in the 550–650 nm range is assigned to the stimulated emission of the S_1 *cis*-keto* formed after the ESIPT reaction. The rise of this stimulated band within the excitation pulse is indicative of an ultrafast ESIPT, as suggested by the gas phase experiments and results reported previously.[40] While this stimulated emission starts to decrease after 400 fs for 390 nm excitation (ESI, 2†), it continues to increase until 800 fs for 266 nm excitation. This difference can be explained by assuming that, upon 266 nm excitation, the formation of the fluorescent S_1 *cis*-keto* species arises from different hot enol* excited conformations *via* several parallel pathways. The decay of stimulated emission can be fitted well with two exponential decay components of 0.5 ± 0.45 and 3.8 ± 0.4 ps time constants. The first contribution has a large error and represents only 2% of the global decay. A 5 ps

monoexponential decay was measured upon 390 nm excitation (ESI, 2†). The shortest component found for 266 nm excitation can be attributed to hot *cis*-keto* species which have a higher probability of forming with 266 nm excitation. The shortening of the main decay with the increasing of the excitation wavelength was already found in the literature and can be explained by a faster formation of the *trans*-keto photo-product with higher energy excitation that competes with *cis*-keto* relaxation to its ground state.[49]

Decays of ground state bleach and absorption bands are difficult to adjust with a global analysis because several species have strongly overlapping spectra with different intensities but similar kinetics. Moreover band shifts are involved. An approximate bi-exponential fit gives two components similar to the decay of spectra after 390 nm excitation: one identical component of about 3.8 ps characterizing the stimulated emission decay and a second component below 2 ps. The time constant and contribution of the second component are wavelength dependent, which indicates the contribution and overlap of enol*, *cis*-keto*, *trans*-keto, unstable *trans*-enol and twisted-enol forms. The pure transient spectra and corresponding time-dependent concentrations obtained for the four components extracted during the MCR-ALS resolution are shown in Fig. 8. The constraints applied during the resolution are the same as those used previously for SAOMe. The fitting error was lof = 2.69% in that case. It was not possible to extract pure spectra for *cis*-keto*, twisted-enol and *trans*-keto photo-products from MCR analysis. However the comparison of the different spectra and the analysis of their respective time-dependent concentration profiles allows us to discuss their growth and decay characteristic times. The first spectrum which appears is the red one, characterized by a broad positive absorption in the 350 to 600 nm domain and a maximum at 400 nm. In comparison with SAOMe this spectrum can be assigned to S_1 enol*. Its time-dependent concentration profile decay function is adjusted by a 550 fs monoexponential kinetics and can be assigned to the competing enol rotation isomerisation and ESIPT processes. A second (green) spectrum grows within the excitation pulse but after that the enol* spectrum has started to decay. The species associated with this green spectrum, which shows the characteristic stimulated emission band, are mainly the *cis*-keto* species arising from ESIPT. Their decay (3 ps) coincides with the growth of a third (blue) spectrum which shows the contribution of the unstable *trans*-enol, an absorption band peaking at 390 nm, and the 480 nm absorption band related to the *trans*-keto photo-product. The main rising contribution (fitting time constant of 1.5 ps) of this blue spectrum is attributed to the formation of the *trans*-keto photo-product. Finally the last (black) spectrum is characteristic of the final *trans*-keto photo-product after the decay of the unstable *trans*-enol. Thus, its growth mainly coincides with the decay of the 390 nm maximum of the blue spectrum (fitting time constant of 16 ps).

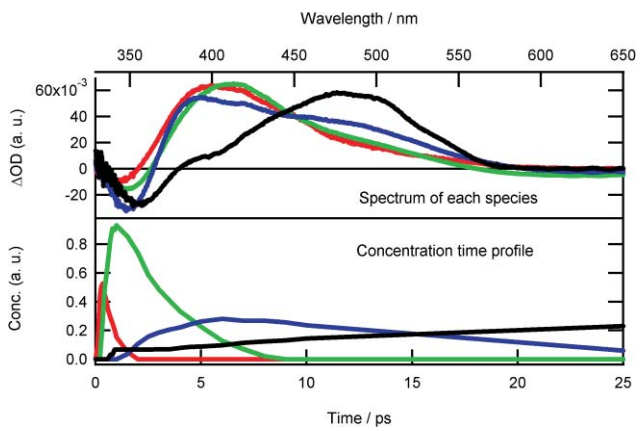

Fig. 8 (Top) Spectra and (bottom) time-dependent concentration profiles obtained from MCR-ALS for transient absorption spectra of SAOH in acetonitrile for different time delays after 266 nm excitation.

C Experimental section

C.1 Materials

Chemical products 2-hydroxybenzylideneaniline (salicylidene aniline or SAOH) and *N*-(2-methoxybenzylidene)aniline (SAOMe) and solvents were used as received (Aldrich).

C.2 Theoretical calculations

The ground state geometries and the force field for the two molecules were studied with the DFT method with the B3LYP functional and 6-31G+(d,p) basis. The excited singlet electronic states, S_1 of the two molecules were calculated with the configuration interaction single method (CIS). A correction of ~1 eV was used for the excitation energies for the two molecules. Our calculations were in accordance with previous ones on SAOH molecule.[48,53]

C.3 Absorption (fluorescence) spectroscopy

C.3.1 Stationary absorption and fluorescence spectroscopy. UV-visible absorption spectra were recorded on a Varian Cary 5 in transmission mode. Spectrophotometric grade solvents were used. The fluorescence excitation spectra were recorded using a FluoroMax3 (Jobin Yvon Horiba) and emission was corrected for the spectral sensitivity of the instrument.

C.3.2 Nanosecond transient absorption spectroscopy (nanosecond laser flash photolysis experiments). Nano- to microsecond transient absorption experiments were performed using a laser flash photolysis apparatus. Excitation pulses at 355 nm and 266 nm (7–8 ns, 1 mJ) were provided by a 20 Hz Nd:YAG laser (DIVA II, Thales laser). The probe light was provided by a Xe lamp (XBO 150W/CR OFR, OSRAM). Samples were contained in a quartz cell (10 mm × 10 mm section) at an adjusted concentration (~10^{-4} mol dm^{-3}) to get an OD value of about 1.0 at the pump excitation wavelength. The transmitted light was dispersed by a monochromator (Horiba Jobin-Yvon, iHR320) and analyzed with a photomultiplier (R1477-06, Hamamatsu) coupled to a digital oscilloscope (LeCroy 454, 500 MHz). The experiment was repeated for different wavelengths of the monochromator and transient spectra were afterwards reconstructed. The quantum yield for the formation of the transient species can be estimated by comparing the differential absorbance value at the maximum for the ground state bleach of the studied compounds and for the triplet state of benzophenone knowing their stationary absorption

coefficients and by taking account that the formation of the triplet state of benzophenone is one.

C.3.3 Femtosecond time-resolved spectroscopy.

C.3.3.1 Transient absorption experimental set up. The femtosecond transient absorption set up has already been described elsewhere.[57,58] Briefly, in our experiments, a 1 kHz Ti:sapphire laser system (Coherent oscillators and a BM Industries re-generative amplifier) delivered 100 fs (0.8 mJ) pulses at 780 nm and 800 nm. Pump pulse was set at 390 nm and 266 nm by frequency doubling and tripling the fundamental beam respectively. The pump pulse energy at the sample was 6 μJ with a diameter of about 0.5 mm (3 mJ cm^{-2}). The white light continuum probe beam was generated by focusing the fundamental beam in a 1 mm CaF_2 rotating plate. The pump–probe polarization configuration was set at the magic angle (54.7°) and the probe pulse was delayed in time relative to the pump pulse using an optical delay line (Microcontrol Model, precision 0.1 μm). The white light continuum was split into a probe beam (with pump) and a reference beam (without pump). The transmitted light of the probe and reference beams was recorded on two different channels of a multichannel spectrograph equipped with a CCD camera (Princeton Instrument) and the transient spectra were computed. The transient absorption measurements covered a 400–750 nm (390 nm excitation) and 320–650 nm (266 nm excitation) spectral range and a 0–5 ns temporal range. The optical density variation ΔOD accuracy was ±0.001 (before averaging) in the spectral range of the experiments. Sample solution (absorbance of 0.8, about 10^{-3} M) was circulating in a flow cell equipped with 1 mm thick CaF_2 windows and characterized by a 2 mm optical path length. The instrumental response function (IRF, about 200 fs and 300 fs for 390 nm and 266 excitation nm respectively) was assimilated to the pump–probe cross-correlation signal obtained by measuring the two photon absorption signal in acetonitrile and ethanol taking into account cell windows dispersion. The transient absorption intensity was displayed as differential absorption and the spectral data at one time delay were measured 4500 times and averaged. All experiments were carried out at 294 ± 2 K. Throughout the paper, we assumed that the temporal resolution did not depend on the wavelength. All experimental data were corrected from the GVD using a procedure proposed by Nakayama *et al.*[59]

C.3.3.2 Gas-phase experimental set up. The experimental setup devoted to gas phase studies had been described in a previous paper.[54] Briefly, the molecules of interest were mixed and compressed in a graphite pill that was introduced in an oven. A pulsed supersonic expansion of helium as carrier gas was blowing through the oven to create a molecular beam. In the present case, the oven was kept at room temperature since the vapour pressure of the molecules of interest were high enough.

The molecular beam went through a skimmer to reach the laser interaction region. Femtosecond lasers were provided by the European facility SLIC/LUCA. In the present paper, the pump laser wavelength was 266 nm, and the probe laser, either 792 nm or 399 nm. The laser cross-correlation time was 95 fs. The ions created are dispersed in mass by a time-of-flight spectrometer.

C.4 Data analysis

Assuming that properties of a multicomponent system may be modeled as additive contributions of the spectroscopic properties of k components weighted by their concentration, a series of transient spectra was decomposed according to eqn (1), in matrix notation.

$$\mathbf{D} = \mathbf{C}\mathbf{S}^{\mathbf{T}} + \mathbf{E} \quad (1)$$

The data matrix **D**, of dimensions $m \times n$, contained transient spectra collected at successive time delay points as rows and time decay traces at every wavelength as columns. The matrix **C**, of dimensions $m \times k$, contained time-dependent concentration profiles of the k pure contributions at m delays and the matrix $\mathbf{S}^{\mathbf{T}}$, of dimensions $k \times n$, the corresponding transient spectra at n wavelengths. The matrix **E** of dimensions $m \times n$ contained the residuals not explained by the k components. Multivariate curve resolution–alternating least squares (MCR-ALS) algorithm aimed at decomposing data according to the linear model given in eqn (1). A detailed description of the method could be found in references 51, 52, 55, 56, 60 and 61; only the main points of the procedure are given.

The method proceeded first by estimating the number of components (transient species) contributing to the variance of the observable raw data **D** using singular values decomposition. Then alternating constrained least-squares optimization of eqn (1) was started by taking **D** and initial estimates of **C** (or $\mathbf{S}^{\mathbf{T}}$). Constraints could be defined as any mathematical or chemical property that the time-dependent concentration profiles and/or spectra had to obey. Applying adequate constraints gave physical meaning to the resolved profiles. For femtosecond absorption spectroscopy data, suitable constraints could be, for example, non-negativity and unimodality (only one maximum in the profile) for the time-dependent concentration profiles, as they were expected to be positive and correspond to a growth-decay shape. The quality of the analysis was assessed from the lack of fit (lof) which was evaluated from the difference between the raw data and the reproduced data. Convergence was achieved when the difference between two consecutive iterations was below a threshold or calculation stops when the number of iterations exceeded a defined value.

All the calculations were performed in Matlab 7.1 (The Matworks, Massachusetts, USA). For MCR-ALS, routines were freely available on the web at the following address http://www.ub.edu/mcr/welcome.html.

D Conclusions

The study presented here enabled us for the first time to undertake a complete overview of the photo-dynamics processes of the best known photochromic salicylidene aniline (SAOH). Two competitive processes were observed after photo-excitation: on one hand, an excited state rotational isomerisation yielding a twisted-enol isomer and, on the other hand, ESIPT followed by a *cis–trans* isomerisation to get a *trans*-keto photo-product. Both processes were observed using ultrafast time-resolved experiments in the gas phase and in acetonitrile after 266 nm excitation. The attribution of all intermediate species was achieved by comparison with the reactivity of the methylated derivative of salicylidene aniline, SAOMe, which can only undergo enol rotation. It showed that proton transfer and rotation of enol* occurred in SAOH within 100 fs (gas phase) as predicted by recent quantum dynamical simulation.[48] Nanosecond transient absorption results showed

that excitation in the first excited state (355 nm) led in majority to ESIPT photo-products with a quantum yield of 14% for the formation of the *trans*-keto photo-product, while excitation in the higher excited state (266 nm) led in majority to enol rotation photo-products with a quantum yield of 23% for the formation of the twisted-enol. Data analysis allowed the extraction of overlapping species for SAOMe and showed that two species are formed: one unstable *trans*-enol (formation within 1.5 ps) which relaxed in few tens of ps to the *trans*-enol and the second was the twisted-enol (observed by nanosecond transient absorption experiments) formed within 500 fs and which relaxed within 1 s. For SAOH, the same unstable *trans*-enol was observed with a similar time scale of formation and decay. However due to the absorption of the *trans*-keto photo-product it was not possible to distinguish the signature of the twisted-enol except in the nanosecond data. It was then assumed that the time constant formation of the twisted-enol was similar to the one measured for SAOMe. Scheme 1 could be then completed with a third deactivation channel from the enol* to the unstable *trans*-enol form (Scheme 2). Finally a caution should be taken in regards to previously published results for SAOH about the decay of positive transient absorption band in the 400–550 nm domain (ESI, 2†).[37] Our current results on SAOMe and SAOH showed that the enol rotation process and formation of different enol isomers (twisted-enol and unstable *trans*-enol) were in fact involved. It was not possible to extract all the species and analyze carefully their formation and decay time constants. Future investigations involving calculations of excited states geometries for SAOH and SAOMe and other experiments such as sub-picosecond time-resolved IR are in progress and should provide more detailed information on the nature of the intermediate species and their dynamics.

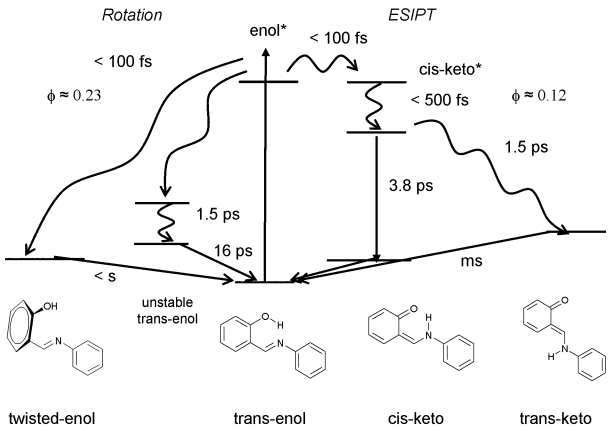

Scheme 2 Overall photoinduced processes for SAOH after 266 nm excitation. Time constant values are taken from solution experiments except for the shortest ones (<100 fs) for which gas phase experiments are used. The formation quantum yields of the *trans*-keto and the twisted enol are also given.

Acknowledgements

The autors are happy to thank the CNRS for fundings through the GDRI 93 PHENICS. LP thanks the ANR for funding the gas phase project through the contract #ANR-09-JCJC-0090-01 (CHROMADYNE).

References

1 *Photochromism*, ed. G. H. Brown, Wiley-Interscience, New York, NY, 1971.
2 *Organic Photochromic and Thermochromic Compounds*, ed. J. C. Crano and R. J. Guglielmetti, Plenum, New York, NY, 1998.
3 *Photochromism: Molecules and Systems*, ed. H. Dürr and H. Bouas-Laurent, Elsevier, Amsterdam, The Netherlands, 1990.
4 M. Irie, Photochromism: Memories and switches - Introduction, *Chem. Rev.*, 2000, **100**, 1683–1683.
5 P. Dedecker, J. Hofkens and J. I. Hotta, Diffraction-unlimited optical microscopy, *Mater. Today*, 2008, **11**, 12–21.
6 M. Heilemann, P. Dedecker, J. Hofkens and M. Sauer, Photoswitches: Key molecules for subdiffraction-resolution fluorescence imaging and molecular quantification, *Laser Photonics Rev.*, 2009, **3**, 180–202.
7 S. W. Hell, Far-field optical nanoscopy, *Science*, 2007, **316**, 1153–1158.
8 *Ultrafast Hydrogen Bonding Dynamics and Proton Transfer Processes in the Condensed Phase (Understanding Chemical Reactivity)*, ed. T. Elsaesser and H. J. Bakker, Kluwer Academic Publishers, Dordrecht, The Netherlands, 2002.
9 K. Amimoto and T. Kawato, Photochromism of organic compounds in the crystal state, *J. Photochem. Photobiol., C*, 2005, **6**, 207–226.
10 E. Hadjoudis and I. M. Mavridis, Photochromism and thermochromism of Schiff bases in the solid state: structural aspects, *Chem. Soc. Rev.*, 2004, **33**, 579–588.
11 A. Plaquet, M. Guillaume, B. Champagne, L. Rougier, F. Mancois, V. Rodriguez, J. L. Pozzo, L. Ducasse and F. Castet, Investigation on the second-order nonlinear optical responses in the keto-enol equilibrium of anil derivatives, *J. Phys. Chem. C*, 2008, **112**, 5638–5645.
12 F. M. Raymo, R. J. Alvarado, S. Giordani and M. A. Cejas, Memory effects based on intermolecular photoinduced proton transfer, *J. Am. Chem. Soc.*, 2003, **125**, 2361–2364.
13 M. Sliwa, S. Letard, I. Malfant, M. Nierlich, P. G. Lacroix, T. Asahi, H. Masuhara, P. Yu and K. Nakatani, Design, synthesis, structural and nonlinear optical properties of photochromic crystals: Toward reversible molecular switches, *Chem. Mater.*, 2005, **17**, 4727–4735.
14 M. Sliwa, N. Mouton, C. Ruckebusch, S. Aloise, O. Poizat, G. Buntinx, R. Metivier, K. Nakatani, H. Masuhara and T. Asahi, Comparative Investigation of Ultrafast Photoinduced Processes in Salicylidene-Aminopyridine in Solution and Solid State, *J. Phys. Chem. C*, 2009, **113**, 11959–11968.
15 J. Harada, T. Fujiwara and K. Ogawa, Crucial role of fluorescence in the solid-state thermochromism of salicylideneanilines, *J. Am. Chem. Soc.*, 2007, **129**, 16216–16221.
16 P. Chen, R. Lu, P. C. Xue, T. H. Xu, G. J. Chen and Y. Y. Zhao, Emission Enhancement and Chromism in a Salen-Based Gel System, *Langmuir*, 2009, **25**, 8395–8399.
17 E. Hadjoudis, S. D. Chatziefthimiou and I. M. Mavridis, Anils: Photochromism by H-transfer, *Curr. Org. Chem.*, 2009, **13**, 269–286.
18 M. Ziolek, G. Burdzinski and J. Karolczak, Influence of Intermolecular Hydrogen Bonding on the Photochromic Cycle of the Aromatic Schiff Base N,N′-Bis(salicylidene)-p-phenylenediamine in Solution, *J. Phys. Chem. A*, 2009, **113**, 2854–2864.
19 M. Ziolek and I. Sobczak, Photochromism and hydrolysis of aromatic Schiff base N,N'-bis(salicylidene)-p-phenylenediamine (BSP) studied in heterogeneous environments, *J. Inclusion Phenom. Macrocyclic Chem.*, 2009, **63**, 211–218.
20 K. Johmoto, A. Sekine, H. Uekusa and Y. Ohashi, Elongated Lifetime of Unstable Colored Species by Intermolecular Hydrogen Bond Formation in Photochromic Crystals, *Bull. Chem. Soc. Jpn.*, 2009, **82**, 50–57.
21 M. D. Cohen and G. M. J. Schmidt, Photochromy and Thermochromy of Anils, *J. Phys. Chem.*, 1962, **66**, 2442–2446.
22 M. D. Cohen and S. Flavian, Topochemistry. 25. Absorption Spectra of Some N-Salicylideneanilines and Related Anils in Solution, *J. Chem. Soc. B*, 1967, 321–328.
23 R. Nakagaki, T. Kobayashi, J. Nakamura and S. Nagakura, Spectroscopic and Kinetic Studies of Photochromism of N-Salicylideneanilines and Related Compounds, *Bull. Chem. Soc. Jpn.*, 1977, **50**, 1909–1912.
24 P. F. Barbara, P. M. Rentzepis and L. E. Brus, Photochemical Kinetics of Salicylidenaniline, *J. Am. Chem. Soc.*, 1980, **102**, 2786–2791.
25 D. Higelin and H. Sixl, Spectroscopic Studies of the Photochromism of N-Salicylideneaniline Mixed-Crystals and Glasses, *Chem. Phys.*, 1983, **77**, 391–400.

26 R. S. Becker, C. Lenoble and A. Zein, A Comprehensive Investigation of the Photophysics and Photochemistry of Salicylideneaniline and Derivatives of Phenylbenzothiazole Including Solvent Effects, *J. Phys. Chem.*, 1987, **91**, 3509–3517.

27 E. Hadjoudis, M. Vittorakis and I. Moustakali-Mavridis, Photochromism and thermochromism of schiff bases in the solid state and in rigid glasses, *Tetrahedron*, 1987, **43**, 1345–1360.

28 E. Hadjoudis, Photochromic and Thermochromic Anils, *Mol. Eng.*, 1995, **5**, 301–337.

29 T. Sekikawa and T. Kobayashi, Femtosecond Fluorescence Study of the Substitution Effect on the Proton Transfer in Thermochromic Salicylideneaniline Crystals, *J. Phys. Chem. A*, 1997, **101**, 644–649.

30 T. Sekikawa, T. Kobayashi and T. Inabe, Femtosecond Fluorescence Study of Proton-Transfer Process in Thermochromic Crystalline Salicylideneanilines, *J. Phys. Chem. B*, 1997, **101**, 10645–10652.

31 S. Mitra and N. Tamai, Femtosecond spectroscopic study on photochromic salicylideneaniline, *Chem. Phys. Lett.*, 1998, **282**, 391–397.

32 J. Harada, H. Uekusa and Y. Ohashi, X-ray analysis of structural changes in photochromic salicylideneaniline crystals. Solid-state reaction induced by two-photon excitation, *J. Am. Chem. Soc.*, 1999, **121**, 5809–5810.

33 S. Mitra and N. Tamai, A combined experimental and theoretical study on the photochromism of aromatic anils, *Chem. Phys.*, 1999, **246**, 463–475.

34 N. Otsubo, C. Okabe, H. Mori, K. Sakota, K. Amimoto, T. Kawato and H. Sekiya, Excited-state intramolecular proton transfer in photochromic jet-cooled N-salicylideneaniline, *J. Photochem. Photobiol., A*, 2002, **154**, 33–39.

35 S. Mitra and N. Tamai, Dynamics of photochromism in salicylideneaniline: A femtosecond spectroscopic study, *Phys. Chem. Chem. Phys.*, 2003, **5**, 4647–4652.

36 M. Ziolek, J. Kubicki, A. Maciejewski, R. Naskrecki and A. Grabowska, Excited state proton transfer and photochromism of an aromatic Schiff base. Pico- and femtosecond kinetics of the N,N′-bis(salicylidene)-p-phenylenediamine (BSP), *Chem. Phys. Lett.*, 2003, **369**, 80–89.

37 M. Ziolek, J. Kubicki, A. Maciejewski, R. Naskrecki and A. Grabowska, An ultrafast excited state intramolecular proton transfer (ESPIT) and photochromism of salicylideneaniline (SA) and its "double" analogue salicylaldehyde azine (SAA). A controversial case, *Phys. Chem. Chem. Phys.*, 2004, **6**, 4682–4689.

38 T. Asahi, H. Masuhara, K. Nakatani and M. Sliwa, Photochromic dynamics of salicylidene aniline in solid state by using femtosecond transient absorption spectroscopy, *Mol. Cryst. Liq. Cryst.*, 2005, **431**, 541–548.

39 M. Ziolek, G. Burdzinski, K. Filipczak, J. Karolczak and A. Maciejewski, Spectroscopic and photophysical studies of the hydroquinone family of photochromic Schiff bases analyzed over a 17-orders-of-magnitude time scale, *Phys. Chem. Chem. Phys.*, 2008, **10**, 1304–1318.

40 W. Rodriguez-Cordoba, J. S. Zugazagoitia, E. Collado-Fregoso and J. Peon, Excited state intramolecular proton transfer in schiff bases. Decay of the locally excited enol state observed by femtosecond resolved fluorescence, *J. Phys. Chem. A*, 2007, **111**, 6241–6247.

41 A. Senier and F. G. Shepheard, Studies in Phototropy and Thermotropy. Part I. Arylidene-, and Naphtylidene-amines, *J. Chem. Soc. Trans.*, 1909, **95**, 1943–1955.

42 A. Senier, F. G. Shepheard and R. Clarke, Studies in Phototropy and Thermotropy. Part III. Arylideneamines, *J. Chem. Soc. Trans.*, 1912, **101**, 1950–1958.

43 C. Curran and E. P. Chaput, Electric Moments of Ortho-Substituted Phenols and Anisoles. 3. Nitriles and Anils, *J. Am. Chem. Soc.*, 1947, **69**, 1134–1137.

44 A. W. Baker and A. T. Shulgin, Intramolecular Hydrogen Bonds to Pi-Electrons and Other Weakly Basic Groups, *J. Am. Chem. Soc.*, 1958, **80**, 5358–5363.

45 R. Destro, A. Gavezzotti and M. Simonetta, Salicylideneaniline, *Acta Crystallogr., Sect. B: Struct. Crystallogr. Cryst. Chem.*, 1978, **34**, 2867–2869.

46 D. G. Anderson and G. Wettermark, Photoinduced Isomerizations in Anils, *J. Am. Chem. Soc.*, 1965, **87**, 1433–1438.

47 M. Ottolenghi and D. S. McClure, Photochromism. 2. Photochemistry of Salicylideneaniline, *J. Chem. Phys.*, 1967, **46**, 4620–4629.

48 J. M. Ortiz-Sanchez, R. Gelabert, M. Moreno and J. M. Lluch, Electronic-structure and quantum dynamical study of the photochromism of the aromatic Schiff base salicylideneaniline, *J. Chem. Phys.*, 2008, **129**, 214308.

49 C. Okabe, T. Nakabayashi, Y. Inokuchi, N. Nishi and H. Sekiya, Ultrafast excited-state dynamics in photochromic N-salicylideneaniline studied by femtosecond time-resolved REMPI spectroscopy, *J. Chem. Phys.*, 2004, **121**, 9436–9442.

50 W. H. Lawton and E. A. Sylvestre, Self Modeling Curve Resolution, *Technometrics*, 1971, **13**, 617–633.

51 R. Tauler, Multivariate curve resolution applied to second order data, *Chemom. Intell. Lab. Syst.*, 1995, **30**, 133–146.

52 A. de Juan and R. Tauler, Multivariate curve resolution (MCR) from 2000: Progress in concepts and applications, *Crit. Rev. Anal. Chem.*, 2006, **36**, 163–176.

53 M. Z. Zgierski and A. Grabowska, Photochromism of salicylideneaniline (SA). How the photochromic transient is created: A theoretical approach, *J. Chem. Phys.*, 2000, **112**, 6329–6337.

54 L. Poisson, K. D. Raffael, B. Soep, J. M. Mestdagh and G. Buntinx, Gas-phase dynamics of spiropyran and spirooxazine molecules, *J. Am. Chem. Soc.*, 2006, **128**, 3169–3178.

55 S. Aloise, C. Ruckebusch, L. Blanchet, J. Rehault, G. Buntinx and J. P. Huvenne, The benzophenone $S_1(n,\pi^*) \rightarrow T_1(n,\pi^*)$ states intersystem crossing reinvestigated by ultrafast absorption spectroscopy and multivariate curve resolution, *J. Phys. Chem. A*, 2008, **112**, 224–231.

56 C. Ruckebusch, S. Aloise, L. Blanchet, J. P. Huvenne and G. Buntinx, Reliable multivariate curve resolution of femtosecond transient absorption spectra, *Chemom. Intell. Lab. Syst.*, 2008, **91**, 17–27.

57 G. Buntinx, R. Naskrecki and O. Poizat, Subpicosecond transient absorption analysis of the photophysics of 2,2′-bipyridine and 4,4′-bipyridine in solution, *J. Phys. Chem.*, 1996, **100**, 19380–19388.

58 B. Moine, J. Rehault, S. Aloise, J. C. Micheau, C. Moustrou, A. Samat, O. Poizat and G. Buntinx, Transient absorption studies of the photochromic behavior of 3H-naphtho[2,1-b]pyrans linked to thiophene oligomers *via* an acetylenic junction, *J. Phys. Chem. A*, 2008, **112**, 4719–4726.

59 T. Nakayama, Y. Amijima, K. Ibuki and K. Hamanoue, Construction of a subpicosecond double-beam laser photolysis system utilizing a femtosecond Ti: sapphire oscillator and three Ti: sapphire amplifiers (a regenerative amplifier and two double passed linear amplifiers), and measurements of the transient absorption spectra by a pump–probe method, *Rev. Sci. Instrum.*, 1997, **68**, 4364–4371.

60 C. Ruckebusch, M. Sliwa, J. Rehault, P. Naumov, J. P. Huvenne and G. Buntinx, Hybrid hard- and soft-modelling applied to analyze ultrafast processes by femtosecond transient absorption spectroscopy: Study of the photochromism of salicylidene anilines, *Anal. Chim. Acta*, 2009, **642**, 228–234.

61 N. Mouton, M. Sliwa, G. Buntinx and C. Ruckebusch, Deconvolution of femtosecond time-resolved spectroscopy data in multivariate curve resolution. Application to the characterization of ultrafast photoinduced intramolecular proton transfer, *J. Chemom.*, 2010, in press.